Int. J. Electrochem. Sci., 17 **(2022)** Article Number: 220750, doi: 10.20964/2002.07.39

International Journal of
ELECTROCHEMICAL
SCIENCE
www.electrochemsci.org

Flower-like nickel-cobalt aluminum composite prepared by hydrothermal method and its application as electrocatalyst for oxygen evolution reaction

Yiwen Zhang[1,2], *Haitao Liu*[1,2], *Chunyong Zhang*[1,2 *], *Zhe Li*[1,2], *Haoyu Wang*[1,2]

[1] Jiangsu Key Laboratory of Precious Metal Chemistry and Technology, Jiangsu University of Technology, Changzhou, 213001, China
[2] School of Chemistry and Environmental Engineering, Jiangsu University of Technology, Changzhou, 213001, China
[*] E-mail: zhangcy@just.edu.cn

Received: 12 March 2022 / *Accepted:* 29 April 2022 / *Published:* 6 June 2022

As we know, the benchmark electrocatalysts for OER in alkaline solution are RuO_2 and IrO_2; however, the high cost, scarcity and instability of these metal oxides prevent their full utilization in OER processes. In consequence, developing non-noble-metal electrocatalysts with low-cost and earth-abundant for efficient and durable oxygen evolution reaction (OER) is highly desirable for sustainable energy development in the future. In this paper, the flower-like nickel-cobalt aluminum alloy was synthesized by hydrothermal method using aluminum foam as base material and mixed with cobalt and nickel salts. At the same time, XRD, XPS, SEM, TEM and electrochemical tests were studied in this paper. Specifically, in 1 M KOH, we found that Ni-S-CoAl-4:1(Co/Ni=4:1) has the best OER performance, this electrode requires a low overpotential of 285 mV at 50 mA cm^{-2} and a small Tafel slope of 60 mV dec^{-1}. This work provides a promising OER catalyst materials with high efficiency and low cost for large-scale electrochemical applications.

Keywords: Aluminum (Al) foams; Oxygen evolution reaction; Cobalt and nickel salts; Electrochemical performance

1. INTRODUCTION

With the development of economy and social progress, the demand for energy is increasing day by day, resulting in a large amount of energy consumption and serious pollution to the environment, energy and environmental problems are becoming more and more prominent [1-2]. It is urgent to develop a clean and sustainable energy [3]. Hydrogen energy is a kind of clean energy with high energy density, wide source and no pollution, it has been widely considered as one of the promising substitutes for fossil

fuels to meet the world's growing energy needs in the future, which has attracted wide attention from all over the world and is known as the ultimate energy in the 21st century [4]. The proposal of China's carbon neutrality target means that green and low-carbon will become an important indicator of energy structure transformation. Therefore, lithium ion battery, sodium ion battery, potassium ion battery, electrolytic water and other new energy technologies for energy storage or conversion have broad development prospects [5]. Among the available hydrogen energy production methods, water electrolysis (oxygen evolution reaction/hydrogen evolution reaction) is a green and economical method by converting electricity into chemical energy [6-8]. Since OER process has slower reaction kinetics and higher overpotential which is the main limiting factor for water splitting [9-10]. Thus, efficient electrocatalysts with high catalytic activity are always required to promote the OER process [11-13].

Nowadays, noble metal-based materials such as Ru, Ir and their alloys have been considered the ideal electrocatalysts for OER processes [14-16]. Nevertheless, their broad-scale applications are greatly impeded by their high costs and rare abundance in the earth [17-21]. Consequently, as alternative selections, it is important to explore high-activity, low cost, environmentally benign and earth-abundant electrocatalysts for OER in place of the aforementioned noble metals [22]. Up to now, a variety of low-cost alternatives to catalyze OER have been investigated, including metal oxides[23-25],hydroxides[26-27], chalcogenides [28-29],phosphates [30] and perovskites [31-32]. As optional materials, Non-precious materials have attracted a lot of attention. In particular, the addition of transition metal such as Ni, Co, Fe, Mn, which can extremely affect the combined strength and thus affect the OER Performance [33-35]. In addition, studies have shown that bimetal compounds were tender to bring better electrochemical performance for OER than single metal compounds. Interestingly, both Ni and Co are abundant elements and are always present together in the earth.

Foam metal is a kind of material with rapid development in current material science. It is composed of metal skeleton and internal holes. A large number of holes in foam metal make it has special functions different from compact metal and becomes a new material with both structure and function, which greatly expands the research field and application scope of porous materials. Common foam metals include aluminum, nickel and their alloys. Aluminum (Al) foam, as one of the classical porous materials, it has become the most widely used foam metal because of its ultra-light, easy manufacturing and low cost. It is a new kind of functional material, which is a non-uniform material composed of matrix metal and pores accounting for more than 70% of the volume. Aluminum foam has excellent physical properties, chemical properties, mechanical properties and recyclability. With the development of various performance research, aluminum foam materials as structural materials and functional materials, are more and more widely used in environmental protection and other application fields. Due to its excellent conductivity, aluminum foam can be widely used as electrode framework material for new batteries such as nickel-zinc batteries and double-layer capacitors. At present, aluminum foam has been tried out by many nickel-zinc battery manufacturers and put into batch use. At the same time, aluminum foam is expected to be widely used as the electrode collector of double electric layer capacitor. In addition, aluminum foam as electrode material for electrolytic recovery of aluminum-containing wastewater, also has a very broad prospect. In many organic chemical reactions, people try to use aluminum foam with large specific surface area directly instead of punching aluminum plate, used as

catalyst for the chemical reaction; as a carrier for photocatalytic air purification, aluminum foam has also been used successfully.

In the current research status of aluminum foam, aluminum foam matrix composites are lightweight porous materials prepared by adding particles or fibers into the aluminum matrix. The addition of reinforcing phase is beneficial to improve the comprehensive performance of aluminum foam. In addition, porous structures have been widely used due to their rich electrochemical activity edge sites and high surface areas which greatly improve their catalytic activity and stability [36]. Specifically, less stable elements etched by alkaline etching produce porous electrodes on the surface, which further optimized the electronic structure of the active site and increased the number of electrocatalytic sites, respectively [37-41]. For example, Liu et al. A 3d metal vacancy solid solution nanowall array was synthesized by selective alkaline etching and phosphorization strategies on the surface of aluminum atoms. The electrocatalytic activity of OER is excellent and the stability of the mesoporous catalytic active site is abundant with a large number of metal defects on the surface of the structure. Therefore, the method for the preparation of porous structures is a promising method to improve the catalytic activity of electrocatalysts.

In this study, the main idea was to use Ni and Co salts in combination with aluminum foams to produce Ni-S-CoAl composites which can effectively electrocatalyze OER in alkaline solution through hydrothermal applications. The physical properties of Ni-S-CoAl composites were characterized by Scanning Electronic Microscopy (SEM), Energy Dispersive System (EDS) and X-Ray Diffraction (XRD), respectively, suggesting that the flower-like nickel-cobalt aluminum alloy is formed with uniform distribution of Ni and Co. The catalytic performance of its electrocatalytic OER was studied.

2. EXPERIMENTAL SECTION

2.1. Materials

$Ni(NO_3)_2 \cdot 6H_2O$, $Co(NO_3)_2 \cdot 6H_2O$, $CO(NH_2)_2$, NH_4F and Na_2S were purchased from Aladdin. Al foam with a thickness of 1 mm was purchased from Kunshan Guangjiayuan New Material Co., LTD and used as the substrate. Ethanol (C_2H_5OH) and Potassium hydroxide (KOH) were obtained from Sinopharm Chemical Reagent Co., Ltd. All the chemicals were analytical grade and used without further purification. Deionized water was used throughout the experiment.

2.2. Substrate pretreatment

Tailored Al foams (1 cm ×2 cm) were cleaned with acetone by ultrasonication for 30 min and immersed in 0.5 M/L hydrochloric acid for 5minutes. Then, Al foams soaked in HCl were rinsed several times with deionized water and ethanol solution and saved in ethanol solution.

2.3. Synthesis of CoAl

$Co(NO_3)_2 \cdot 6H_2O$(3.3 mmol), NH_4F(13.3 mmol),urea (20.0 mmol) were dissolved in deionized water (70 mL) by stirring to obtain a transparent solution. Then, the solution was transferred into a 100 mL stainless steel autoclave with several pre-treated Al foams, maintained at 120 °C for 24 h and then naturally cooled to room temperature. The pink sediment and Al foams were taken out and washed repeatedly with deionized water and ethanol solution. Thereupon CoAl foams were obtained.

2.4. Synthesis of S-CoAl

The CoAl composites were placed into a 100 mL stainless steel autoclave with a solution containing 70 mL sodium sulfide (0.51 mM) and kept under the condition of 100 °C for 24 h. After cooling down to room temperature, the S-CoAl composites were collected and rinsed several times with deionized water and ethanol solution.

2.5. Synthesis of Ni-S-CoAl

$Ni(NO_3)_2 \cdot 6H_2O$(0.4,0.8,1.65,3.3mmol) were dissolved in deionized water (70 mL) respectively by stirring. The S-CoAl composites were placed into a 100 mL stainless steel autoclave with the solution prepared above, maintained at 120 °C for 24 h and then naturally cooled to room temperature. The products were taken out and washed repeatedly with deionized water and ethanol solution.

2.6. Material characterization

The scanning electron microscope (SEM) images and energy dispersive X-ray spectroscopy (EDS) images of the composite foams were performed by a scanning electron microscopy. X-ray diffraction (XRD, PW3040/60, PANalytical B.V, and the scanning range of 2θ is 5° to 90°) was used to determine the substance contained in the composite foams. The states of the elements were analyzed by X-ray photoelectron spectroscopy (XPS, Thermo Scientific K-Alpha). The transmission electron microscopic (TEM) images were obtained by Transmission Electron Microscope (TEM, JEOL JEM 2100).

2.7. Electrochemical measurements

The whole electrochemical measurements including CV, LSV, TAFEL and EIS were measured by electrochemical workstation (CHI760E, China) using a conventional three-electrode system. The prepared material was used as working electrode, a platinum gauze electrode and saturated calomel electrode were used as the counter electrode and the reference electrode respectively. The exposed geometric area of the working electrode for electrochemical test was about 1×1 cm^2. All the electrochemical tests were conducted in 1 mol/L KOH aqueous electrolyte. The cyclic voltammetry was

tested by varying the scan rate from 2 to 7 mV/s. The polarization curves were plotted by linear sweep voltammetry (LSV) at the scanning rate of 1 mV/s in 1 M KOH aqueous solution. All of the potentials were converted to reverse hydrogen electrode (RHE) by the equation E (RHE) = E (Hg/HgO) + 0.921 V and were corrected with 95% iR compensation unless otherwise stated. Tafel data were collected by galvanostatic method [42-43]. The electrochemical impedance spectroscopy (EIS) measurements were measured in the range from 100 kHz to 0.01Hz.

3. RESULTS AND DISCUSSION

The morphologies of the samples were characterized by scanning electron microscopy (SEM), the SEM images of the obtained composites are shown in Fig. 1. As shown in Fig. 1A, with the addition of cobalt salts, it can be observed that the Co nanoparticles were loaded on Al foams in a flower-like form with needle-like leaves.

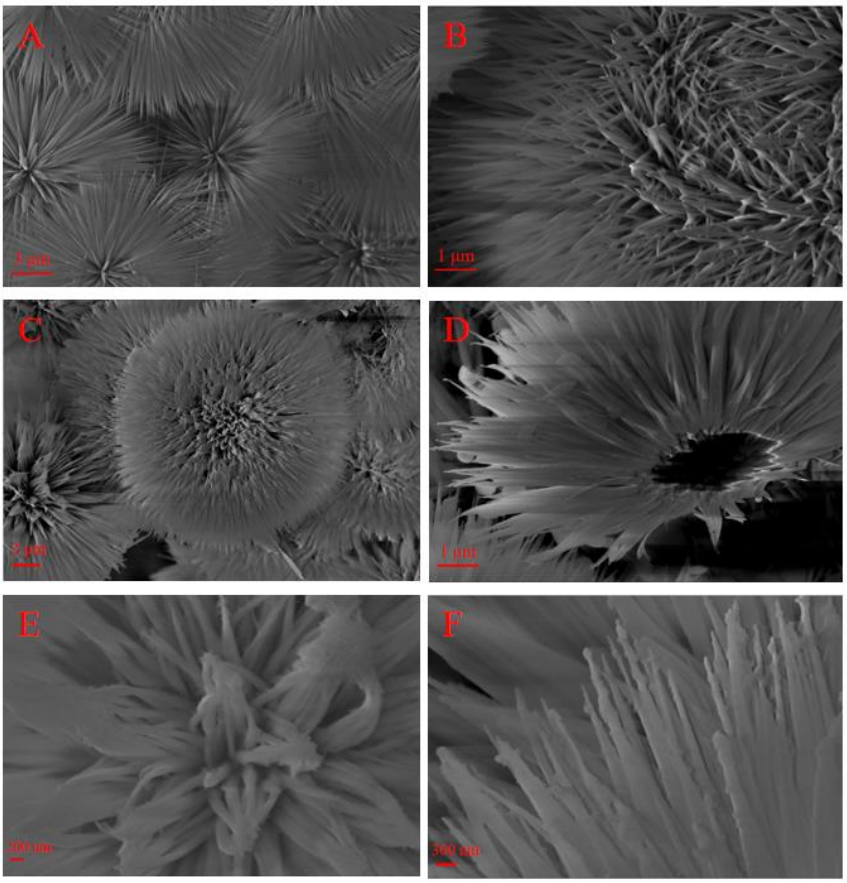

Figure 1. (A) SEM image of CoAl, (B) SEM images of S-CoAl, (C-F) SEM images of Ni-S-CoAl.

The Co nanoparticles were deposited on the surface of reticulated Al foams closely. Fig. 1B show that the S-CoAl nanosheets become thicker, and it still possesses flower-like morphology. Meanwhile,

after adding nickel salt and cobalt salt at the same time, the flower-like morphology of the Ni-S-CoAl is well maintained, moreover, the roughness and thickness of each nanosheet increased (Fig. 1C, D, E, F).

The diffractograms of the X-ray diffraction patterns of as-prepared samples were shown in Fig. 2. Fig. 2A shows XRD patterns of Al foam, CoAl and S-CoAl. The diffraction peaks of samples can be matched with CoAl (JCPDS card no. 51-0045) and AlOOH (JCPDS card no. 99-0044). From Fig. 2B, the vital diffraction peaks of Ni at 2θ values of 44.507 °, 51.846 °, 76.370 ° are indexed to the (111), (200), (220) planes, respectively. In addition, there are no other impurity phases were detected, indicating high purity of these samples [44]. Using XPS technology to further analyze the surface chemical composition and the valence of the element of the Ni-S-CoAl. From the XPS survey spectra in Fig. 3A, it can be concluded that the material is composed of S, O, Ni, Al and Co. The XPS spectrum of Ni-S-CoAl for Co 2p is displayed in Fig. 3B, it can be seen that the partial peak spectrum corresponding to Co 2p includes two main peaks of Co $2p_{3/2}$ and Co $2P_{1/2}$ and two satellite peaks (Sat.). The peaks with binding energy of 781.2 and 797.2 eV are characteristic peaks of Co^{2+}. The peaks with binding energies of 778.7 and 793.5 eV belong to the characteristic peaks of Co^{3+}. In addition, the corresponding satellite peaks appear at 786.6 and 802.8 eV [45]. The presence of Co^{3+} with oxygen vacancy could effectively promote the adsorption of H_2O and OER intermediates, and hence improve the OER activity [46-47]. Fig.3C shows the partial peak spectra corresponding to Ni 2p. The two main peaks are corresponding to Ni $2p_{3/2}$ and Ni $2p_{1/2}$ respectively. For Ni $2p_{3/2}$, it can be divided into two characteristic peaks, Ni^{2+} and Ni^{3+} are 855eV and 856.1eV respectively. However, the XPS peak at the binding energy of 856.1 eV was the contribution of Ni^{3+} caused by hydroxylating nickel oxide on the surface. Similarly, the other peaks were located at two peaks with binding energies of 861.3 eV and 879.2 eV, respectively, which were the satellite peaks of Ni 2p XPS [48-49]. As observed, Fig.3D shows the peak spectra of O 1S, which are located at 531.8 eV, 531.3 eV and 530.5 eV respectively.

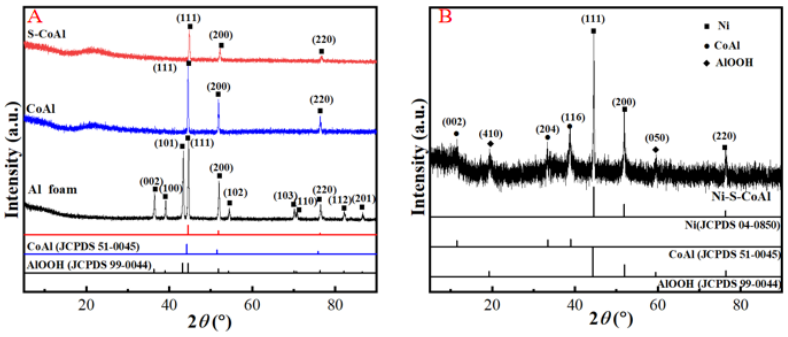

Figure 2. XRD patterns of (A) Al foam, CoAl and S-CoAl, (B) Ni-S-CoAl.

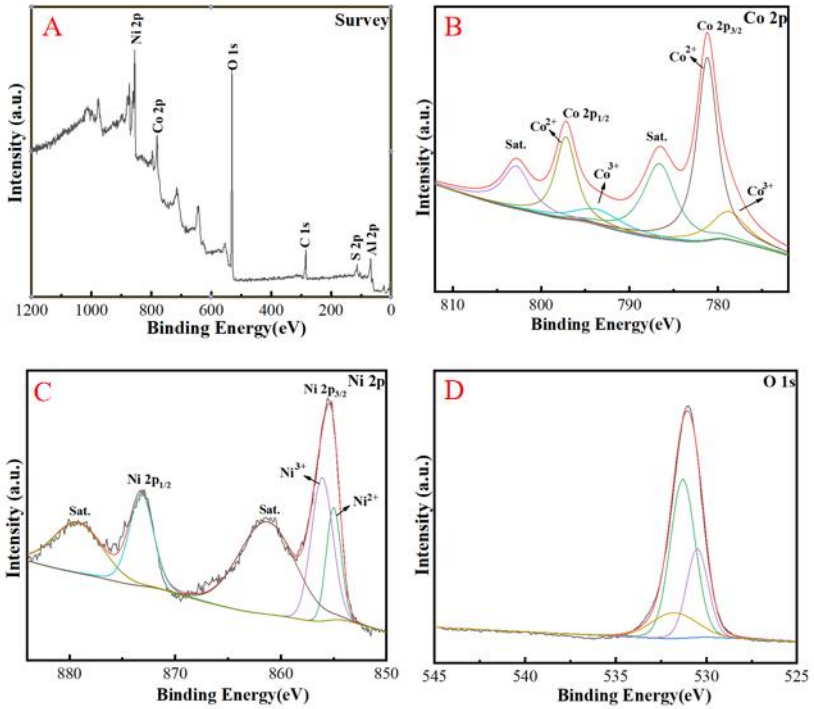

Figure 3. The full survey XPS spectrum of (A) Ni-S-CoAl and (B-D)XPS spectra for Co 2p, Ni 2p and O 1s of Ni-S-CoAl.

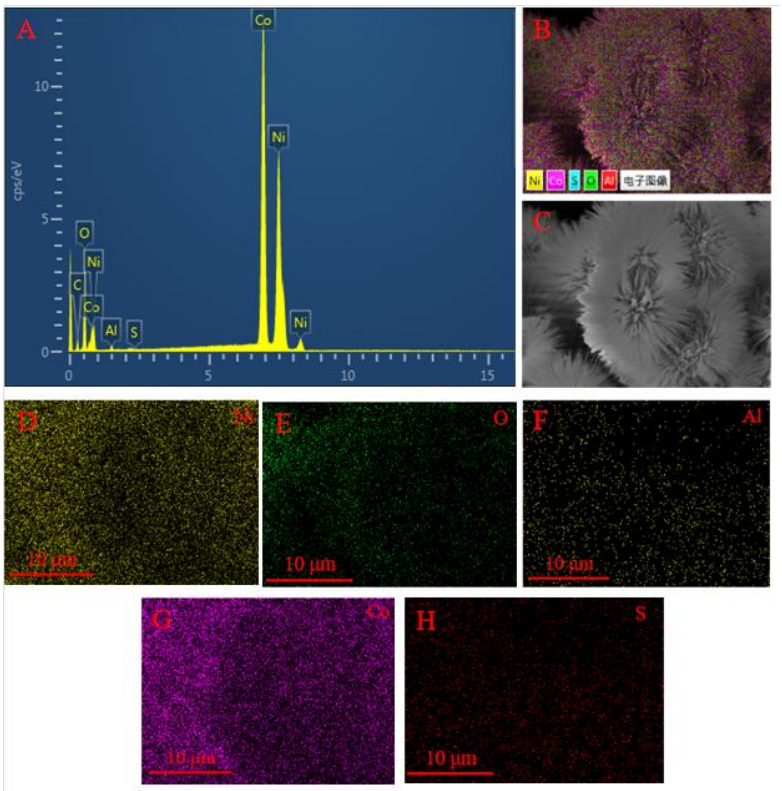

Figure 4. (A) The EDS spectra of Ni-S-CoAl, (B-C) SEM mapping images of Ni-S-CoAl, (D-H) The EDS elemental mapping images of the Ni, O , Al, Co and S in the Ni-S-CoAl.

In order to further determine the existence of O, Ni, Co, Al and S in the Ni-S-CoAl, energy dispersive spectrometer (EDS) full mapping was completed. As shown in Fig. 4A, the EDS full spectrum reveals that the composite contains O, Ni, Co, Al and S elements. All elements were derived from the obtained sample. Fig.4 (B-C) shows the SEM mapping images of Ni-S-CoAl. As shown in Fig. 4(D-H), it can also confirmed the formation of Ni-S-CoAl, which showed that O, Ni, Co, Al and S elements were evenly distributed in the whole nanocomposites. Table 1 shows the elements distribution in the Ni-S-CoAl, O, Ni, Co, Al and S are distributed in the Ni-S-CoAl, and values of 35.00 wt% (O), 26.90 wt% (Ni), 34.10 wt% (Co), 0.40 wt% (Al) and 3.60 wt% (S) were determined, and the corresponding atomic ratio are 65.30%, 13.70%, 17.30%, 0.40% and 3.30% respectively.

Table 1. The elements distribution in the Ni-S-CoAl

Element	Weight percent/%	Atomic percent/%
O	35.00	65.30
Ni	26.90	13.70
Co	34.10	17.30
Al	0.40	0.40
S	3.60	3.30
Amounts	100	100

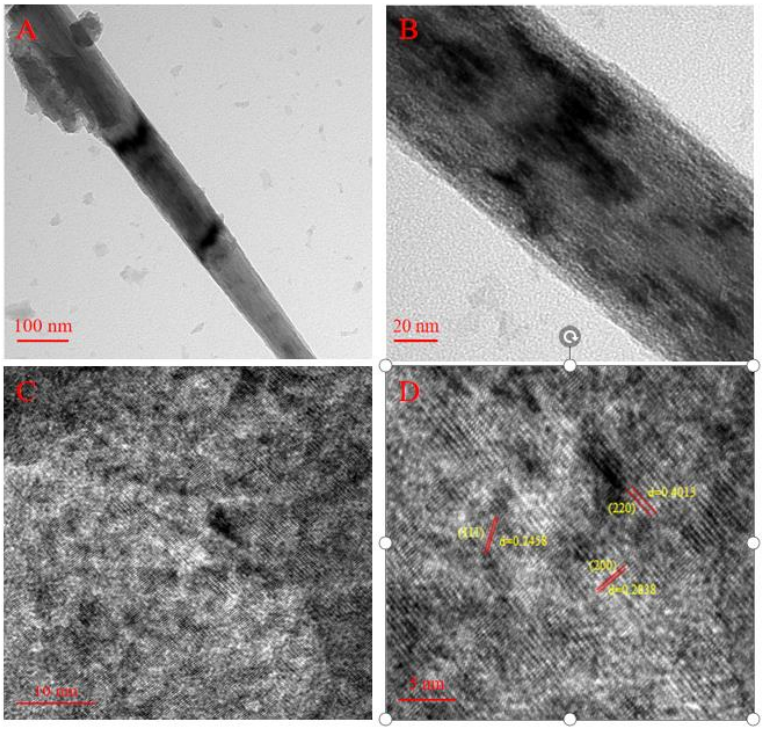

Figure 5. (A-C) High magnification TEM images for Ni-S-CoAl, (D) HRTEM image for Ni-S-CoAl.

The microstructure of Ni-S-CoAl was further investigated by TEM and HRTEM. TEM and HRTEM images of Ni-S-CoAl are shown in Fig.5. The TEM images further proved the needle-like

structure of leaves, corresponding to the SEM results. From Fig. 5D, the lattice spacing d=0.2458 nm, 0.2838 nm and 0.4013 nm index to (111), (200) and (220) of spinel type, respectively. Meanwhile, the results of TEM and HRTEM are consistent with the XRD pattern, as is discussed above in Fig. 2.

Table 2 compares the synthesized electrocatalysts in this paper with similar OER electrocatalysts.

Table 2. Comparison of oxygen evolution reaction of Ni-S-CoAl in this work with previously reported studies.

Electrocatalyst	Test Solution	Tafel slope/ (mV dec^{-1})	Overpotential/ (mV)	Current density/ (mA cm^{-2})	Reference
ES-CoAl-LDH	1 M KOH	63	270	10	[50]
$CoNi_xS_y$/NCP	0.1 M KOH	71	280	10	[51]
Co_3O_4	1 M KOH	76	311	50	[52]
NiFe	1 M NaOH	126.12	292	10	[53]
Ni-S-CoAl	1 M KOH	60	285	50	This work

To better identify the effect of the relative ratio of Co and Ni, Ni-S-CoAl samples with different mole ratios of Co/Ni (8:1, 4:1, 2:1, 1:1) were synthesized. The OER electrochemical properties of the catalysts were tested in 1 M KOH solution. When the current density is 50 mA/cm^2, the corresponding overpotentials of CoAl, S-CoAl, Ni-S-CoAl-8:1(Co/Ni=8:1), Ni-S-CoAl-4:1(Co/Ni=4:1), Ni-S-CoAl-2:1(Co/Ni=2:1) and Ni-S-CoAl-1:1(Co/Ni=1:1) are 400, 370, 352, 285, 325 and 295 mV, respectively. The results suggest the Ni-S-CoAl-4:1(Co/Ni=4:1) generates numerous active sites, which greatly improves its OER catalytic activity.

Fig. 6 B shows Tafel curves which reflect the rate of oxygen evolution and can be obtained from the polarization curves, the value of Tafel indicates the OER kinetics of the corresponding electrocatalyst. Tafel slope of Ni-S-CoAl-4:1 (60 mv/dec) significantly lower than the tafel slopes of contrast samples, table the electrocatalytic OER reaction rate of Ni-S-CoAl-4:1(Co/Ni=4:1) is faster.

In order to estimate the ECSA of electrocatalytic materials under the water oxidation reaction processes, the Cdl from cyclic voltammetry curves in non-faraday current area has been measured. As shown in Fig. 6C, the Cdl value for Ni-S-CoAl-4:1(Co/Ni=4:1) is largest, indicating that Ni-S-CoAl-4:1(Co/Ni=4:1) possesses larger electro-chemical surface area and thus improving the OER activity [54].

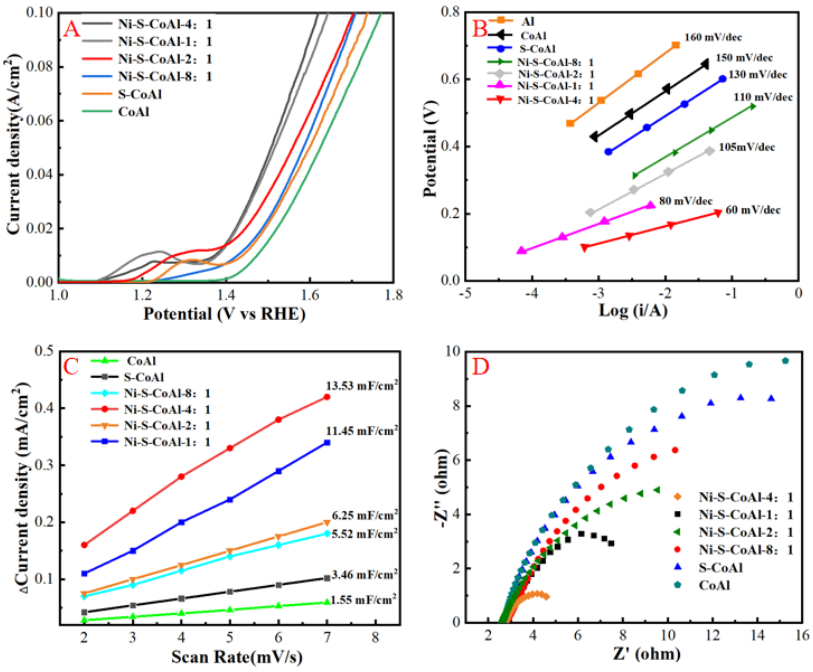

Figure 6. (A) LSV curves of different catalysts, (B) Corresponding Tafel slopes from the OER LSV curves, (C) The plots of ΔJ versus scan rates for different electrocatalysts, (D) The electrochemical impedance spectroscopy (EIS) Nyquist plots of different catalysts.

In order to further evaluate the charge transfer abilities and electrocatalytic activity of OER, the electrocatalytic OER process was studied by mean of electrochemical impedance spectroscopy (EIS) [55]. Electrochemical impedance spectroscopy (EIS) is regarded as one of the important means to explain the catalytic activity [56]. As shown in Fig. 6D, the charge transfer impedance diagram (Nyquist diagram) of samples were obtained, obviously, Ni-S-CoAl(4:1) (Co/Ni=4:1) is smaller than other contrast samples, demonstrating that the faster charge transfer rate of Ni-S-CoAl(4:1) (Co/Ni=4:1) during the electrochemical OER process, and thus it has better OER catalytic activity, which is consistent with LSV curves and Tafel slopes.

4. CONCLUSION

In summary, porous aluminum foams as base materials, the samples were successfully prepared by doping with metal nickel salt and cobalt salt by a simple hydrothermal method. By controlling the mole ratio of nickel to cobalt, we found that Ni-S-CoAl-4:1(Co/Ni=4:1) has the best OER performance, overpotential of 285 mV at 50 mA cm^{-2}, Tafel slope of 60 mV dec^{-1}, which is more excellent than other samples. Compared with the electrochemical properties, Ni-S-CoAl-4:1(Co/Ni=4:1) has a larger electrochemical active surface area, faster charge transfer rate, so has better OER catalytic activity than other samples. In this paper, the results are useful for the further synthesis of more efficient non-noble metal OER Catalyst materials have important guiding significance.

DECLARATION OF COMPETING INTEREST
The authors declare that we have no conflicts of interest.

ACKNOWLEDGEMENTS
This work was financially supported by Postgraduate Research & Practice Innovation Program of Jiangsu University of Technology (XSJCX21_74), National Natural Science Foundation of China (grant no. 31800495), Natural Science Foundation of Jiangsu Province (grant no. BK20181040).

References

1. Z. Wang, S. Zeng, W. Liu, X. Wang, Q. Li, Z. Zhao and F. Geng, *ACS Appl. Mater. Interfaces*, 9 (2017) 1488-14959.
2. S. Cobo, J. Heidkamp, P. A. Jacques, J. Fize, V. Fourmond, L. Guetaz, B. Jousselme, V. Ivanova, H. Dau and S. Palacin, *Nat. Mater.*, 11 (2012) 802-807.
3. X. Chen, C. Jiang and Y. Zhang, *J Membr Sci*, 544 (2017) 397-405.
4. Y. Jiao, Y. Zheng and M. Jaroniec, *Chem. Soc. Rev.*, 44 (2015) 2060-2086.
5. X. Liu, W. Zhang and S. Liu, *J. Energy Chem.*, 53 (2021) 192-196.
6. L. D. Wickramasinghe, R. Zhou, R. Zong, K. J. Gagnon and R. P. Thummel, *J. Am. Chem. Soc.*, 137 (2015) 13260-13263.
7. Y.-H. Kim, H. O. Kim, E. J. Baek, R. Kurita, H.-J. Cha, Y. Nakamura and H. Kim, *Nat. Commun.*, 6 (2015) 8678.
8. T. Faunce, S. Styring, M. R. Wasielewski, G. W. Brudvig, A. W. Rutherford, J. Messinger, A. F. Lee, C. L. Hill, H. Degroot and M. Fontecave, *Energy Environ. Sci.*, 6 (2013) 1074-1076.
9. P. Lyu and P. Natchtigall, *Catal Today*, 345 (2020) 220-226.
10. M. Okamura, M. Kondo, R. Kuga, Y. Kurashige, T. Yanai, S. Hayami, V. K. K. Praneeth, M. Yoshida, K. Yoneda, S. Kawata and S. Masaoka, *Sci. Nat.*, 530 (2016) 465-468.
11. J. Lim, S. Yang, C. Kim, C. W. Roh, Y. Kwon, Y. T. Kim and H. Lee, *Chem. Commun.*, 52 (2016) 5641-5644.
12. R. R. Rao, M. J. Kolb, N. B. Halck, A. F. Pedersen, A. Mehta, H. You, K. A. Stoerzinger, Z. Feng, H. A. Hansen, H. Zhou, L. Giordano, J. Rossmeisl, T. Vegge, I. Chorkendorff, I. E. L. Stephens and Y. Shao-Horn, *Energy Environ. Sci.*, 10 (2017) 2626-2637.
13. L. Gloag, T. M. Benedetti, S. Cheong, R. F. Webster, C. E. Marjo, J. J. Gooding and R. D. Tilley, *Nanoscale*, 10 (2018) 15173-15177.
14. E. Fabbri, A. Habereder, K. Waltar, R. Kötz and T. J. Schmidt, *Catal. Sci. Technol.*, 4 (2014) 3800-3821.
15. N. T. Suen, S. F. Hung, Q. Quan, N. Zhang, Y. J. Xu and H. M. Chen, *Chem. Soc. Rev.*, 46 (2017) 337-365.
16. L. S. Bezerra and G. Maia, *J. Mater. Chem. A.,* 8 (2020) 17691-17705.
17. M. Gong, W. Zhou, M.-C. Tsai, J. Zhou, M. Guan, M.-C. Lin, B. Zhang, Y. Hu, D.-Y. Wang and J.Yang, *Nat.Commun*, 5 (2014) 1-6.
18. P. Du, R. Eisenberg, *Energy Environ. Sci.*, 5(2012) 6012-6021.
19. E. Petkucheva, G. Borisov, E. Lefterefterova, J. Heiss, U. Schnakenberg and E. Slavcheva, *Int J Hydrogen Energ*, 43 (2018) 16905-16912.
20. R. Forgie, G. Bugosh, K. C. Neyerlin, Z. Liu and P. Strasser, *Electrochem Solid ST*, 13 (2010) B36−B39.
21. H. N. Nong, L. Gan, E. Willinger, D. Teschner and P. Strasser, *Chem. Sci.*, 5 (2014) 2955-2963.
22. B. K. Martini and G. Maia, *Electrochim. Acta*, 8 (2021) 138907.
23. W. Gao, Z. Xia, F. Cao, J. C. Ho, Z. Jiang and Y. Qu, *Adv Funct Mater*, 28 (2018) 1706056.

24. H. Jin, J. Wang, D. Su, Z. Wei, Z. Pang and Y. Wang, *J. Am. Chem. Soc*, 137(2015) 2688-2694.
25. K. L. Pickrahn, S. W. Park, Y. Gorlin, H. B. R. Lee, T. F. Jaramillo and S. F. Bent, *Adv. Eng. Mater.*, 2 (2012) 1269-1277.
26. Z. Zhao, P. S. Lamoureux, A. Kulkarni and M. Bajdich, *ChemElectroChem*, 11 (2019) 3423-3431.
27. Y. Qin, F. Wang, J. Shang, M. Iqbal, A. Han, X. Sun, H. Xu and J. Liu, *J. Energy. Chem.*, 43 (2020) 104-107.
28. K. C. Majhi, P. Karfa and R. Madhuri, *Electrochim Acta*, 318 (2019) 901-910.
29. Y. Du, S. Khan, X. Zhang, G. Yu, R. Liu, B. Zheng, R. Nadimicherla, D. Wu and R. Fu, *Carbon*, 149 (2019) 144-151.
30. D. Zhao, Q. Shao, Y. Zhang and X. Huang, *Nanoscale*, 10 (2018) 22787-22791.
31. R. N. Singh, J. P. Singh and A. Singh, *J. Power Sources*, 33 (2008) 4260-4264.
32. K. J. May, C. E. Carlton, K. A. Stoerzinger, M. Risch, J. Suntivich, Y. L. Lee, A. Grimaud and Y. Shao-Horn, *J. Phys. Chem. Lett.*, 3 (2012) 3264-3270.
33. X. F. Lu, L. F. Gu, J. W. Wang, J. X. Wu, P. Q. Liao and G. R. Li, *Adv. Mater.*, 29 (2017) 1604437.
34. L. Han, S. J. Dong and E. K. Wang, *Adv. Mater.*, 28 (2016) 9266-9291.
35. M. S. Burke, S. H. Zou, L. J. Enman, J. E. Kellon, C. A. Gabor, E. Pledger and S. W. Boettcher, *J. Phys. Chem. Lett.*, 6 (2015) 3737-3742.
36. H. Sun, X. Xu, Z. Yan, X. Chen, F. Cheng, P. S. Weiss and J. Chen, *Chem. Mater.*, 29 (2017) 8539-8547.
37. W. Cheng, H. Zhang, X. Zhao, H. Su, F. Tang, J. Tian and Q. Liu, *J. Mater. Chem. A*, 6 (2018) 9420-9427.
38. Y. Zeng, L. Chen, R. Chen, Y. Wang, C. Xie, L. Tao, L. Huang and S. Wang, *J. Mater. Chem. A*, 6 (2018) 24311-24316.
39. Y. Zeng, Y. Wang, G. Huang, C. Chen, L. Huang, R. Chen and S. Wang, *Chem. Commun.*, 54 (2018) 1465-1468.
40. J. Xie, X. Zhang, H. Zhang, J. Zhang, S. Li, R. Wang, B. Pan and Y. Xie, *Adv. Mater.*, 29 (2017) 1604765.
41. M. Q. Yang, J. Wang, H. Wu and G. W. Ho, *Small*, 14 (2018) 1703323.
42. P. Manna, J. Debgupta, S. Bose and S. K. Das, *Angew. Chem. Int. Ed.,* 55 (2016) 2425-2430.
43. Y. Wu, Y. Liu, G.-D. Li, X. Zou, X. Lian, D. Wang, L. Sun, T. Asefa and X. Zou, *Nano Energy*, 35 (2017) 161-170.
44. T. Jiang, J. Kong, Y. Wang, D. Meng, D. Wang and M. Yu, *Cryst Res Technol*, 51 (2016) 58-64.
45. X. Feng, Q. Jiao, H. Cui, M. Yin, Q. Li, Y. Zhao, H. Li, W. Zhou and C. Feng, *ACS Appl. Mater. Interfaces*, 10 (2018) 29521-29531.
46. Y. Zeng, L. Chen, R. Chen, Y. Wang, C. Xie, L. Tao, L. Huang and S. Wang, *J. Mater. Chem. A*, 6 (2018) 24311-24316.
47. Y. Wang, C. Xie, Z. Zhang, D. Liu, R. Chen and S. Wang, *Adv. Funct. Mater.*, 28 (2018) 1703363.
48. B. Zhao, X.-K. Ke, J.-H. Bao, C.-L. Wang, L. Dong, Y.-W. Chen and H.-L. Chen, *J. Phys. Chem. C*, 113 (2009) 14440-14447.
49. G. Bai, H. Dai, J. Deng, Y. Liu and K. Ji, *Catal. Commun.*, 27 (2012) 148-153.
50. X. Guo, F. Wu, G. Hao, S. Peng, N. Wang, Q. Li, Y. Hu and W. Jiang, *Dalton Trans.*, 16 (2019) 5214-5221.
51. Y. Zheng, L. Zhang, H. Huang, F. Wang, L. Yin, H. Jiang, D. Wang, J. Yang and G. Zuo, *Int J Hydrogen Energ*, 44 (2019) 27465-27471.
52. D. Tang, Y. Ma, Y. Liu, K.Wang, Z. Liu, W. Li and J. Li, *J. Alloys Compd.*, 893 (2022) 162287.
53. X. Yang, Z. Li, J. Qin, M. Wu, J. Liu, Y. Guo, Y. Ma and F. Feng, *J. Fuel Chem. Technol.*, 49 (2021) 827–834.
54. Y. Zeng, L. Chen, R. Chen, Y. Wang, C. Xie, L. Tao, L. Huang and S. Wang, *J. Mater. Chem. A*, 6 (2018) 24311-24316.
55. B. K. Kang, S. Y. Im and J. Lee, *Nano Res*, 12 (2019) 1605-1611.

56. K. Pandey and P. Yadav, *J. Electroanal. Chem.*, 745 (2015) 88-97.